https://doi.org/10.5194/tc-2022-127
Preprint. Discussion started: 4 October 2022

The Cryosphere Discussions
Open Access
EGU

Sentinel-1 detection of seasonal and perennial firn aquifers in the Antarctic Peninsula

Lena G. Buth[1], Bert Wouters[2,3], Sanne B. M. Veldhuijsen[2], Stef Lhermitte[3], Peter Kuipers Munneke[2], and Michiel R. van den Broeke[2]

[1]Alfred Wegener Institute, Helmholtz Centre for Polar and Marine Research, Bremerhaven, Germany
[2]Institute for Marine and Atmospheric Research, Department of Physics, Utrecht University, Utrecht, the Netherlands
[3]Department of Geoscience & Remote Sensing, Delft University of Technology, Delft, the Netherlands

Correspondence: Lena G. Buth (lena.buth@awi.de), Bert Wouters (b.wouters@uu.nl)

Abstract. In recent years, the existence of firn aquifers in the Antarctic Peninsula (AP) has been confirmed by in-situ observations. Given their importance for understanding the hydrology of the Antarctic ice sheet, a more spatially comprehensive assessment of AP firn aquifers is desirable. The purpose of this study is to map firn aquifers in the AP from space using C-band Synthetic Aperture Radar imagery from ESA's Sentinel-1 mission. These observations enable the detection of firn aquifers at 1 x 1 km^2 resolution. The method presented here is based on quantifying the characteristic, gradual backscatter increase during the (partial) refreezing of the liquid water in the firn layer after the peak melt season. When applied to the available time series, it detects perennial aquifers (existing year-round) for the period 2017 to 2020, as well as seasonal aquifers which do not persist through winter. We acknowledge that the backscatter signature in any given year is indistinguishable for seasonal and perennial aquifers. We detect seasonal firn aquifers in the north and northwest of the AP, as well as on the Wilkins and George VI ice shelves. Only in the north and northwest of the AP, aquifers are detected each year in the observation period, here taken as a proxy for perennial firn aquifers. Both distributions agree with model simulations. Further in situ and modelling studies and longer time series of satellite observations are needed to validate the results of this study.

1 Introduction

The Antarctic Peninsula (AP, Fig. 1) is the mildest and wettest region in Antarctica, with high accumulation rates of up to several metres of water equivalent per year ($\mathrm{w.e.\,y^{-1}}$) on its western side (Fig. 1a), and the highest summer melt rates of the continent, mainly at lower elevations (Fig. 1b; van Wessem et al., 2015; 2017). Situated between two ocean basins that are covered by sea ice for extended periods each year, the AP experiences large natural variability in temperature. In the beginning of this century, the observed rapid warming during the 20th century (Hansen et al., 2010) reversed into a weak cooling trend (Turner et al., 2016). However, under the influence of anthropogenic forcing, the AP is expected to undergo further warming in the long term. With meltwater production expected to increase with future warming (Trusel et al., 2015; Siegert et al., 2019),

https://doi.org/10.5194/tc-2022-127
Preprint. Discussion started: 4 October 2022

it is essential to understand its pathways, as it is known to play a role in ice shelf disintegration (Scambos et al., 2000; van den Broeke, 2005; Scambos et al., 2009; Gilbert and Kittel, 2021). On the Antarctic ice sheet, the fate of surface meltwater is either refreezing, runoff, supraglacial storage in melt ponds or englacial storage in buried meltwater lakes (Lenaerts et al., 2017). Under specific conditions it is also possible that the meltwater percolates through the pore space without refreezing to form firn aquifers, areas of subsurface liquid water storage. Seasonal firn aquifers form during the peak melt season and last for several weeks to months into fall, after which the meltwater refreezes when the cold wave moves from the surface down through the firn in the subsequent winter. An aquifer is called perennial when the refreezing of the aquifer is not yet complete when the next melt season starts. Perennial firn aquifers develop when a favourable combination of high melt and high accumulation rates prevents part of the stored meltwater to refreeze during winter (Kuipers Munneke et al., 2014), after which the aquifer can be recharged in the following summer. On the Greenland ice sheet, extensive perennial firn aquifers have been observed before the start of the melt season using in-situ measurements (e.g. firn cores) as well as ground and airborne radar, most prominently relying on data from the NASA Operation Ice Bridge (OIB) mission (Forster et al., 2014; Miège et al., 2016; Chu et al., 2018), and satellite remote sensing, using Sentinel-1 (S1) C-band radar imagery (Brangers et al., 2020) and L-band brightness temperature measurements from the Soil Moisture Active Passive (SMAP) satellite mission (Miller et al., 2020). Perennial firn aquifers have also been detected in Svalbard (Christianson et al., 2015). The presence of firn aquifers in the Antarctic Peninsula has been confirmed by in situ observations on the Wilkins ice shelf by Montgomery et al. (2020) and on the Müller ice shelf by MacDonell et al. (2021). AP firn aquifers have also been simulated in firn models forced with output of a regional climate model (van Wessem et al., 2021). However, there are currently no published spatially comprehensive observational studies of firn aquifers in Antarctica. This study therefore aims to map firn aquifers in the AP from space, using S1 radar backscatter measurements. A new method is developed, exploiting the dependency of the C-band backscatter signal on the wetness of the firn (Stiles and Ulaby, 1980) and the resulting characteristic delayed backscatter increase after the peak melt season in the presence of firn aquifers. Peak melt season here refers to the summer months December, January and February, acknowledging that melt can occur throughout the year in the AP (Kuipers Munneke et al., 2018). Section 2 presents data and methods, Section 3 results, Section 4 a discussion followed by conclusions in Section 5.

2 Data and Methods

2.1 Preprocessing of Sentinel-1 data

Synthetic Aperture Radar (SAR) Level-1 Ground Range Detected (GRD) images from the Copernicus Sentinel-1 (S1) mission were used to detect the presence of firn aquifers in the AP. S1 measurements of backscatter strength are available since the satellite Sentinel-1A was launched in April 2014. Sufficiently dense data coverage for our purpose was only reached after the launch of Sentinel-1B in April 2016. Consequently, this analysis focuses on the period starting with the melt season in summer 2016/17, using data from the years 2017 to 2020. The radar instruments operate at a centre frequency of 5.405 GHz (C-band), so that clouds and solar illumination conditions do not influence the radar signal. We used acquisitions from the Extra-Wide Swath Mode with a swath of 400 km and a spatial resolution of 20 x 40 m. A preprocessed version of the data was accessed via

https://doi.org/10.5194/tc-2022-127
Preprint. Discussion started: 4 October 2022


The Cryosphere Discussions

the Python API of the Google Earth Engine (Gorelick et al., 2017), where GRD border noise removal, thermal noise removal, radiometric calibration and terrain correction was already applied. The data are available in dual polarisation, here only the band of co-polarized (HH) backscatter measurements (σ_{HH}) are used. The images were reprojected to the Equal-Area Scalable Earth (EASE) Grid 2.0 South (Brodzik et al., 2012) at 1 km resolution. The S1 satellites are each in a 12 day repeat cycle with 175 orbits per cycle. For each satellite pass within one cycle, identified by its relative orbit number (RON), the geometry of the orbiting satellite with respect to the Earth's surface is different, which influences the backscatter measurements and results in a RON-specific bias. This bias was determined pixel-wise by taking the average σ_{HH} of each RON and subtracting the average σ_{HH} of all orbit numbers. Subsequently, the bias was removed for all RONs with at least 50 data points. Data points from remaining RONs were eliminated with the reasoning that for RONs with few data points, the bias cannot be determined accurately, as the average might be influenced by seasonal variability.

2.2 Aquifer detection algorithm

Microwave radar backscatter decreases with increasing wetness of snow, due to the higher absorption and difference in scattering of the radar signal by the liquid water (Stiles and Ulaby, 1980; Shi and Dozier, 1992; Tsai et al., 2019). Using the Snow Microwave Radiative Transfer (SMRT) model (Picard et al., 2018, see Section 2.4), Figure 2 shows the simulated backscatter from an artificial snowpack at the S1 frequency, where the snowpack is defined by an upper snow layer of varying thickness, a snow grain size of 400 $\mu\mathrm{m}$ and density of 200 $\mathrm{kg\,m^{-3}}$, an underlying 1 m thick firn layer of either wet (5 % liquid water content) or dry firn with a grain size of 400 $\mu\mathrm{m}$ and density of 600 $\mathrm{kg\,m^{-3}}$ and several constant layers below. In case of a thin top layer of snow, the wet firn layer causes a clear reduction in backscatter compared to the dry scenario. With increasing thickness of the snow cover, this contrast decreases. Consequently, an important limitation of the S1 aquifer detection method is that the difference in σ_{HH} between dry and wet firn is only distinctive if the wet layer is in the upper few metres of the firn. At a depth of 7 m the difference is already smaller than the S1 radiometric accuracy (3 standard deviations) of 1 dB. Unlike the observations of OIB flights, the S1 data therefore does not allow for a direct measurement of the depth of the water table. Instead, the S1 firn aquifer detection method is based on the temporal evolution of the S1 radar backscatter after the peak melt season. During melt episodes the backscatter signal is low for all locations with snow melt. At locations without significant liquid melt water retention, the immediate refreezing after the melt season results in a quick increase in σ_{HH} up to pre-melt season values within a few days or weeks. In contrast, burial and downward percolation of retained liquid melt water results in a delayed increase of the radar backscatter signal after the peak melt season. In the presence of an underlying perennial firn aquifer, latent heat from partial refreezing and high snow accumulation slow down the refreezing of upper layers (Humphrey et al., 2012; Phillips et al., 2010; Brangers et al., 2020; Kuipers Munneke et al., 2014). This also results in an increase of radar backscatter which is considerably delayed compared to non-aquifer locations. This difference in the σ_{HH} curve over time is used to differentiate firn aquifers from non-firn aquifers. There have been various approaches of quantifying such a delay in signatures for the detection of firn aquifers in Greenland. Brangers et al. (2020) used the difference of S1 radar backscatter near the end of winter to that of early autumn to deduce the presence of firn aquifers, while Miller et al. (2020) fitted a sigmoid curve to L-Band brightness temperature curves. In this study, a new pixel-based approach is introduced as illustrated in Fig. 3. The

https://doi.org/10.5194/tc-2022-127
Preprint. Discussion started: 4 October 2022


The Cryosphere Discussions

mean backscatter σ_{Jan} in the peak melt season between 1 and 15 January, where typically the lowest values are reached, and the mean backscatter in September σ_{Sep}, where values are typically stable on a high level, were recorded. Locations without distinct increase in backscatter after the melt season (σ_{Sep} - $\sigma_{\mathrm{Jan}} \leq 3$ dB) were masked out, as these are considered dry-snow regions without summer melt. The σ_{HH} time series was smoothed using a 15-day centred moving average. The first day of the year at which the smoothed time series reaches 80 % of σ_{Sep} with respect to σ_{Jan} (DOY_{80}) was determined. A threshold was defined such that pixels with $\mathrm{DOY}_{80} \geq 105$ (mid-April) are classified as firn aquifer locations. This threshold was chosen based on the observation that DOY_{80} can be as early as mid-April at locations with the typical monotone increase of σ_{HH} until the beginning of the next summer melt season, which is associated with firn aquifers. When mapping the resulting firn aquifers, noise removal was applied by removing connected areas with 3 or less pixels, corresponding to an area of 3 km^2. The definition of the term "firn aquifer" in the context of this study includes all firn aquifers that are still detectable using S1 by mid-April (15 April, DOY 105). It cannot therefore be excluded that some of the classified aquifers are not perennial but seasonal (Kuipers Munneke et al., 2014), i.e. complete refreezing of the aquifer occurs after mid-April but before the start of the next melt season. As the analysis is based on quantifying the backscatter curve between one summer and the next, starting with the period of typically low backscatter in early January, the beginning of each annually observed period approximately coincides with the beginning of a calendar year. Consequently, we can describe the backscatter evolution following summer melt and the extent of newly formed or refilled aquifers by referring to the corresponding calendar year.

2.3 Firn model and regional climate model

The detected spatial extent of aquifers is compared with results from the latest version of the IMAU Firn Densification Model (IMAU-FDM v1.2A) (Ligtenberg et al., 2011; van Wessem et al., 2021; Veldhuijsen et al., 2022). Using layers of 2 to 15 cm thickness, the semi-empirical IMAU-FDM simulates the transient evolution of a vertical firn column using a Lagrangian layer administration. The model includes parameterizations for heat conduction, dry snow densification, meltwater percolation and refreezing. Meltwater percolation is simulated with the tipping-bucket method, whereby each firn layer has a maximum irreducible water content that decreases with increasing density following Coléou et al. (1999). Any remaining meltwater moves downwards through all layers in a single model timestep, until it refreezes in a layer with sufficient available pore space and if sufficient heat can be extracted. Otherwise, remaining liquid water can be retained up to the maximum irreducible water content. Percolation continues until the pore close-off depth, where the firn layer transitions to impermeable glacier ice, after which instantaneous runoff is assumed. IMAU-FDM is forced at its upper boundary by three-hourly fields of instantaneous surface temperature, 10-m wind speed, accumulation (total precipitation minus sublimation minus drifting snow erosion) and cumulative surface liquid water input (melt plus rain) from the regional atmospheric climate model RACMO2.3p2 (Fig. 1, van Wessem et al., 2018; 2021). RACMO2 has a horizontal resolution over the AP of 5.5 x 5.5 km^2, which also determines the horizontal resolution of IMAU-FDM. IMAU-FDM does not simulate standing water or lateral water flow, so only a qualitative comparison can be made with S1 detected aquifers on the basis of the presence of irreducible liquid water content. When applied over the Greenland ice sheet, a previous version of IMAU-FDM accurately predicted the location of observed (using in situ data and airborne radar) perennial firn aquifers (Forster et al., 2014; Kuipers Munneke et al., 2014; Steger et al., 2017).

https://doi.org/10.5194/tc-2022-127
Preprint. Discussion started: 4 October 2022

2.4 SMRT radiative transfer model

To compare the IMAU-FDM time series of firn aquifers with the observed S1 time series for selected locations (see Fig. 1a), we translated the IMAU-FDM time series of density, temperature and liquid water content into a simulated S1 HH-backscatter time series using the SMRT radiative transfer model (Picard et al., 2018). Therefore, 10-day IMAU-FDM depth profiles of density, temperature and liquid water content with a vertical resolution of 4 cm were converted into a SMRT snowpack, where we assumed an exponential microstructure model with correlation length of 1 mm throughout the profile. This SMRT snowpack was subsequently translated into modelled S1 backscatter using SMRT with S1 settings for frequency (5.405 GHz) and typical incidence angle (30°) and using the Discrete Ordinate and Eigenvalue Solver (DORT).

3 Results

3.1 Sentinel-1 and SRTM backscatter time series at four locations

To demonstrate the advantages and difficulties in the Sentinel-1 (S1) detection method and its validation, Fig. 4 shows time series of relevant observed and modelled parameters at four sample locations (see Fig. 1a) with progressively higher backscatter reduction and (modelled) liquid water content. On Larsen C ice shelf (Fig. 4a), a location with rapid meltwater refreezing and therefore small amounts of retained liquid water, every year the observed backscatter increases rapidly to σ_{Sep} values at the end of the melt season and DOY_{80} remains below the threshold value of 105. As a result, the S1 firn aquifer detection method returns a negative result: no firn aquifer is detected. On George VI, Wilkins and Müller ice shelves in Figs. 4b-d, the increase in observed S1 backscatter is more gradual and extends over longer time periods with the regular occurrence of $\mathrm{DOY}_{80} \geq 105$, meaning that a firn aquifer is detected by S1. The location on Müller ice shelf (Fig. 4d), however, shows higher amounts of retained liquid water and therefore lower backscatter in September and non-uniform backscatter increases. Here, the DOY_{80} threshold might underestimate the presence of aquifers in some years (e.g., 2020).

There is a clear correspondence between the presence of liquid water in IMAU-FDM and the corresponding forward-modelled SMRT S1 backscatter time series on the one hand, and the observed S1 backscatter time series on the other hand. For instance, in the summer of 2020, IMAU-FDM simulates higher liquid water content (LWC), and the modelled SMRT and observed S1 backscatter time series show good correspondence with a more gradual increase in backscatter. However, in the summer of 2019, IMAU-FDM simulates lower liquid water content, and the modelled SMRT backscatter increases quickly after the melt season, whereas the observed S1 backscatter time series only increases gradually. This indicates that IMAU-FDM in combination with SMRT potentially underestimates aquifer presence for some years. Alternatively, the S1 backscatter signal could represent persistent or slowly buried supraglacial lakes, which are features not taken into account by IMAU-FDM.

3.2 Aquifer extent using Sentinel-1 remote sensing data

Figure 5 shows the spatial distribution of the parameter DOY_{80} for 2019 (a) and 2020 (b), the two years with the smallest and largest detected firn aquifer area in the studied period, respectively. Reddish colours represent the locations where DOY_{80}

https://doi.org/10.5194/tc-2022-127
Preprint. Discussion started: 4 October 2022

exceeds the threshold of 105, our definition for the presence of a firn aquifer in that year. In 2019, the detected total aquifer area amounts to 14,109 km^2 and in 2020 to 41,970 km^2. Although the time series are short, a large interannual variability in firn aquifer area is implied, and this suggests that firn aquifers are seasonal in most areas. In 2019, firn aquifers are detected in the coastal regions in the north, northwest and west of the AP. In 2020, there are additional firn aquifer locations on the Wilkins ice shelf as well as on the northern and southern extremities of the George VI ice shelf.

3.3 RACMO2.3p2 climate in aquifer regions

By comparing Figs. 1 and 5, we demonstrate that aquifers are mainly detected in regions where both snow accumulation and snowmelt rates are high, in line with previous studies (Kuipers Munneke et al., 2014). In regions with high snowmelt but relatively low accumulation rates, such as Larsen C ice shelf, aquifers are generally not detected. Fig. 6 quantifies this further by comparing the S1 detected aquifer pattern to the RACMO2.3p2 2017-2020 average fields of accumulation and surface snowmelt. For this we assigned each RACMO2 pixel to bin sizes of 50 $\mathrm{mm\,w.e.\,y^{-1}}$ average snowmelt and 200 $\mathrm{mm\,w.e.\,y^{-1}}$ average accumulation. The colour shows the percentage of S1 detected aquifer occurrences within these bins, for occurrences in all years (a) and occurrence in at least a single year (b) in the period 2017-2020, as a function of average annual surface melt (y-axis) and accumulation (x-axis) for that period. Detected aquifers are clearly located in regions where both surface melt and accumulation rates are high. The figure also reveals that the fraction of detected aquifers generally does not decline with increasing accumulation for a given melt rate. This indicates that the S1 detection method does not fail to detect aquifers in regions with high accumulation rates and the associated fast burial. Firn aquifer occurrence in at least one year (Fig. 6b) is also high in regions with relatively low average melt (50-100 $\mathrm{mm\,w.e.\,y^{-1}}$). This could be associated with a single high-melt year, or model underestimated melt, as climate models have difficulties in accurately estimating surface melt over areas with low surface albedo, such as ponds and meltwater lakes (Hu et al., 2021).

3.4 Comparison with IMAU-FDM liquid water content

The fact that the spatial extent of the S1-detected firn aquifers differs strongly from year to year suggests that seasonal firn aquifers explain a significant part of the interannual variability. But, as stated above, based on the S1 detection method alone we cannot make this distinction between seasonal and perennial firn aquifers. To investigate this further we use the output of a firn model, IMAU-FDM v1.2A, forced with three-hourly output of RACMO2.3p2 for the same period (2017-2020, Fig. 7). For the purpose of this study, we define seasonal firn aquifers to be present in IMAU-FDM as locations where liquid water is present in April (post-summer but pre-winter) but not in the following September (post-winter but pre-summer), and perennial firn aquifers where liquid water is present in both April and the following September. Fig. 7a shows the areas where S1 detects a firn aquifer in at least one of the four years in the period 2017-2020 (blue plus orange in Fig. 7a) or all of the three years with complete coverage (2018-2020, orange). Figs. 7b and c show the occurrence of seasonal (blue) and perennial (orange) firn aquifers in IMAU-FDM, for two definitions of perennial aquifers: in panel (b) we require at least a single September month in the period 2018-2020 to have LWC > 0, in panel (c) we require all three September months to have LWC > 0. The areas of the blue plus orange regions in Fig. 7a (62,680 km^2) and Figs. 7b and c (59,740 km^2) are comparable and also show a similar

https://doi.org/10.5194/tc-2022-127
Preprint. Discussion started: 4 October 2022

spatial distribution: firn aquifers are detected and modelled along the north-western coast of the AP as far south as George VI ice shelf, and along the AP's northeastern coast as far south as (the remainder of) Larsen B ice shelf. The South Shetland Islands show almost complete firn aquifer cover, confirmed by local observations (Jiahong et al., 1998; Travassos and Simoes, 2004; Macheret et al., 2009). Further south, the firn aquifer signals become more restricted to the low-lying island's coastal zones. Furthest south, Alexander Island only has firn aquifers along its northern and western coasts. Extensive firn aquifers are detected and modelled over Wilkins ice shelf but more fragmented coverage and also some discrepancies between the two products are found over George VI, Bach and Larsen C ice shelves. The orange areas in Fig. 7a (aquifers detected in all years by S1, 10,240 km^2) and Figs. 7b (perennial firn aquifers modelled by IMAU-FDM in at last a single year, 16,274 km^2) and c (perennial firn aquifers modelled by IMAU-FDM in all three years, 7,865 km^2) are again comparable in magnitude and spatial patterns. As expected, the total perennial firn aquifer area is much reduced compared to the area of seasonal firn aquifers. The bands of perennial firn aquifers along the AP coast are narrower and more restricted to the lowest-lying regions, and on Wilkins and George VI ice shelves, perennial firn aquifers occur only sporadically.

4 Discussion

4.1 Limitations of the method

The most important limitation of the Sentinel-1 (S1) firn aquifer detection method is that it does not directly measure the liquid water content in the firn. The increase of backscatter over time after the peak melt season can be caused by the wet layer getting buried under fresh snow accumulation, by (partial) refreezing of the wet layer, by further downward percolation of the wet layer or by a combination of these processes. A delay in the backscatter increase cannot be attributed specifically to either of these processes, although Fig. 6 shows that the S1 detection method does still work in regions with fastest burial. While underlying perennial firn aquifers might also be the cause for a delayed signature due to an inhibited refreezing of upper layers, this is not necessarily the case. For this reason, it is currently not possible to distinguish between perennial and seasonal firn aquifers using S1 detection alone. Likewise, it is not possible to quantify the water table depth, firn aquifer thickness or the total amount of liquid water in the firn layer with this method.

Another limitation of the proposed S1 firn aquifer detection method is that it might underestimate the presence of aquifers in regions that still have high amounts of liquid water in the upper 15 m of the firn in September. This may result in lower backscatter in September (σ_{Sep}) and non-uniform backscatter increases (e.g. Müller ice shelf in 2020). In these cases, the DOY_{80} threshold might underestimate the presence of aquifers in some years where the model indicates high liquid water content. This may result in the underestimation of perennial aquifers from the Sentinel-1 data.

In the absence of longer observational time series, it is hard to come up with an observation-based estimate of uncertainties. Obviously, the detected firn aquifer extent is sensitive to the choice of the DOY_{80} threshold: moving the threshold 7 days earlier increases the blue plus orange area in Fig. 6a by 26 % and the orange area by 12 %. Accordingly, shifting the threshold to a date 7 days later decreases the blue plus orange area by 17 % and the orange area by 20 %. During the OIB campaign on Wilkins ice shelf, the water table depth reached values of up to 20 m (Montgomery et al., 2020), which is deeper than

https://doi.org/10.5194/tc-2022-127
Preprint. Discussion started: 4 October 2022

can be detected by S1. Therefore, it is reasonable to assume that choosing a later DOY_{80} threshold implies potentially not detecting perennial firn aquifers which are too deep to still influence the signal after several months. On the other hand, an earlier threshold would include signals from surface meltwater or meltwater in the firn which refreezes soon after the melt events. Our choice of threshold is a compromise between both scenarios and while it gives plausible results, it might cause an under- or overestimation of the firn aquifer extent at certain locations.

No information about the length of the summertime melt season at a specific location is incorporated into the algorithm. The threshold for firn aquifer classification is a fixed date range, which discriminates against locations with a short melt season and does not consider the interannual variability of surface melt dates. An alternative method based on melt duration information based on radiometer (Special Sensor Microwave Imager/Sounder - SMMIS) and scatterometer (Advanced Scatterometer - ASCAT) observations was attempted but rejected as the irregular occurrence of melt events outside of the summer months is difficult to account for. In the current version of the detection algorithm, outliers in the backscatter time series are not eliminated. The outliers are not expected to have a large effect on the estimated total aquifer area, but they might affect the parameter DOY_{80} and thereby influence the classification of individual locations in individual years. This issue should be resolved in future applications.

A further limitation in the S1 firn aquifer detection method is that for some years and some locations in the AP, the amount of data points is not sufficient for this analysis. This issue will become less relevant in the coming years as the amount of data is increasing, although a complication is that Sentinel-1B has failed since December 2021 with no guarantee of operating again.

The comparison to IMAU-FDM is not perfect, and the simulation of aquifers in IMAU-FDM is hampered by simplifying parameterizations as well as deficiencies in the climate forcing, which is taken from a regional climate model. As examples of missing processes in IMAU-FDM, lateral (horizontal) flow is not included, and the model is currently not simulating standing water over an impenetrable surface (such as thick ice lenses). Instead, liquid water is assumed to percolate all the way to the bottom of the firn column, to the firn-ice interface. There, it is assumed to run off instantaneously, and is thereby removed from the firn column. Likely, this causes IMAU-FDM to systematically underestimate the volume of liquid water in firn aquifers which precludes the use of modelled LWC in a more quantitative comparison.

4.2 Interpretation of results

In spite of the limitations discussed above, there are multiple indications that the S1 firn aquifer detection method presented here provides a reasonable estimate of firn aquifer extent in the AP. Aquifers are detected in regions where they are expected due to high accumulation and melt values according to theoretical considerations (Fig. 6, Kuipers Munneke et al., 2014). Moreover, spatial patterns generally agree well with seasonal and perennial aquifers modelled in IMAU-FDM, giving confidence in both results. This preliminary comparison also suggests that the S1 detection method could be used to establish proxies for seasonal and perennial aquifers, e.g. by imposing that perennial aquifers are detected in a number of consecutive years. Based on this result, perennial aquifers exist in regions where both snow accumulation and snow melt are high, whereas seasonal aquifers are found in regions with high melt but not necessarily high snow accumulation. Comparing the satellite detection results with in-situ measurements on the Wilkins and Müller ice shelves (Montgomery et al., 2020; MacDonell et al., 2021) is complex

https://doi.org/10.5194/tc-2022-127
Preprint. Discussion started: 4 October 2022

as dissimilar quantities in different time scopes are measured. On Wilkins Ice Shelf, the reported aquifer water tables were typically located at 6 to 22 meter the surface in 2014, and IMAU-FDM does not provide indications that the very deep aquifers have been recharged in recent years. At these depths, the radiometric accuracy of the Sentinel-1 backscatter observations becomes too low to reliably detect the presence or absence of an aquifer (see Figure 2). However, knowing that liquid water retention is possible at these locations validates the assumption that firn aquifers were present in at least some of the years. Further analysis of OIB flight measurements would be useful for comparison as they provide information on the firn aquifer water table on a larger scale. Especially collecting measurements before the peak melt season would be valuable as they allow detection of perennial firn aquifers which are more robustly defined than seasonal aquifers. Currently the OIB-based water table data are only available for November 2014 (Montgomery et al., 2020), a moment for which S1 based aquifer detection is not yet possible. For a comparison of the same period, S1 data from January 2014 would be necessary, whereas the first S1 satellite (Sentinel-1A) was only launched in April 2014. Finally, it is noteworthy that the existence of perennial firn aquifers at the grounding line and the presence of extensive floating ice shelves appear to be mutually exclusive on both sides of the AP (Fig. 7). This suggests that perennial firn aquifers play an important role in ice shelf viability and demise: if a perennial firn aquifer develops around the grounding line or on the ice shelf, it is a precursor for collapse. An exception is Wilkins ice shelf, but it is well known that this ice shelf has partly disintegrated in recent years (Braun et al., 2009).

5 Conclusions

This study presents a method for mapping Antarctic Peninsula (AP) firn aquifers from space using Sentinel-1 (S1), based on a delayed increase of SAR backscatter after the peak melt season in the presence of a firn aquifer. In principle, the proposed method cannot distinguish between seasonal firn aquifers (that last for several months before refreezing) and perennial firn aquifers (that survive throughout the winter), as in both cases the backscatter curves can have a similar shape. However, comparing with firn model output suggests that firn aquifer persistence from year to year provides insight in the partitioning of seasonal and perennial aquifers. The total area of S1 detected seasonal firn aquifers in at least one of the four years between 2017 and 2020 amounts to 62,680 km^2, in good agreement with the model seasonal aquifer product (59,740 km^2). The area in which an aquifer was detected in every year between 2018 and 2020 is 10,240 km^2, again in agreement with the model perennial firn aquifer product (7,865 km^2 - 16,274 km^2, depending on how strictly the definition is applied).

Good agreement between satellite and model is also found in the spatial distribution: seasonal firn aquifers are found in the coastal regions in the northwest and north of the AP, on the Wilkins ice shelf and in the north and south of George VI ice shelf. Compared to seasonal aquifers, the perennial firn aquifers along the AP are confined to narrow bands in the lowest-lying areas, and the presence of perennial aquifers on Wilkins and George VI ice shelves is only sporadic. The locations of the detected perennial firn aquifers coincide with regions of high snow accumulation and snow melt, supporting previous studies that these conditions are required for their formation. An interesting finding is that the presence of perennial firn aquifers at the grounding line and extensive floating ice shelves appear to be mutually exclusive, suggesting that perennial firn aquifer development around the grounding line could be a precursor of ice shelf demise. With temperatures in the AP rising in a

https://doi.org/10.5194/tc-2022-127
Preprint. Discussion started: 4 October 2022

future warming climate, increased snowfall/rainfall and surface melt and less refreezing might increase the amount of liquid water in the firn and thereby enhance firn aquifer formation, influencing the stability of ice shelves. It thus remains important to continue observing firn aquifers in the AP. Further studies are needed to validate the presented S1 detection method, and evaluate the IMAU-FDM model results. More in-situ measurements of the firn liquid water content and improved modelling of water transport in firn can help calibrate the demonstrated method and aid to better distinguish perennial from seasonal firn aquifers in the AP.

Code and data availability. The Python code for S1 firn aquifer detection using the Google Earth Engine is published via GitLab (https://gitlab.awi.de/lenbuth/tc-aquifers). IMAU-FDM data as well as maps of DOY_{80} and the corresponding detected aquifer locations for each year can be downloaded from https://doi.org/10.5281/zenodo.7113603 (Buth et al., 2022). Alternatively, the S1 detection results can be accessed in the original resolution as an asset directly in the Google Earth Engine (https://code.earthengine.google.com/?asset=users/lbuth/aquifers_AP). A brief description of the datasets can be found in the GitLab and Zenodo projects.

Author contributions. LB and BW designed the study and the Sentinel-1 experiments and LB carried them out in Google Earth Engine. SV ran the IMAU-FDM model and SL the SRTM model. LB prepared the manuscript with contributions from all co-authors.

Competing interests. MB, BW and SL are members of the editorial board of journal The Cryosphere.

Financial support. Sanne Veldhuijsen, Bert Wouters and Stef Lhermitte acknowledge funding by NWO grant OCENW.GROOT.2019.091.

https://doi.org/10.5194/tc-2022-127
Preprint. Discussion started: 4 October 2022

References

Brangers, I., Lievens, H., Miège, C., Demuzere, M., Brucker, L., and De Lannoy, G. J. M.: Sentinel-1 Detects Firn Aquifers in the Greenland Ice Sheet, Geophysical Research Letters, 47, e2019GL085 192, https://doi.org/10.1029/2019GL085192, 2020.

Braun, M., Humbert, A., and Moll, A.: Changes of Wilkins Ice Shelf over the past 15 years and inferences on its stability, The Cryosphere, 3, 41–56, https://doi.org/10.5194/tc-3-41-2009, 2009.

Brodzik, M. J., Billingsley, B., Haran, T., Raup, B., and Savoie, M. H.: EASE-Grid 2.0: Incremental but Significant Improvements for Earth-Gridded Data Sets, ISPRS International Journal of Geo-Information, 1, 32–45, https://doi.org/10.3390/ijgi1010032, 2012.

Buth, L. G., Veldhuijsen, S. B. M., Wouters, B., Lhermitte, S., and van den Broeke, M. R.: Modelled and Sentinel-1 detected firn aquifers areas in the Antarctic Peninsula, https://doi.org/10.5281/zenodo.7113603, 2022.

Christianson, K., Kohler, J., Alley, R. B., Nuth, C., and van Pelt, W. J. J.: Dynamic perennial firn aquifer on an Arctic glacier, Geophysical Research Letters, 42, 1418–1426, https://doi.org/10.1002/2014GL062806, 2015.

Chu, W., Schroeder, D. M., and Siegfried, M. R.: Retrieval of Englacial Firn Aquifer Thickness From Ice-Penetrating Radar Sounding in Southeastern Greenland, Geophysical Research Letters, 45, 11,770–11,778, https://doi.org/10.1029/2018GL079751, 2018.

Coléou, C., Xu, K., Lesaffre, B., and Brzoska, J.-B.: Capillary rise in snow, Hydrological Processes, 13, 1721–1732, https://doi.org/10.1002/(SICI)1099-1085(199909)13:12/13<1721::AID-HYP852>3.0.CO;2-D, 1999.

Forster, R. R., Box, J. E., van den Broeke, M. R., Miège, C., Burgess, E. W., van Angelen, J. H., Lenaerts, J. T. M., Koenig, L. S., Paden, J., Lewis, C., Gogineni, S. P., Leuschen, C., and McConnell, J. R.: Extensive liquid meltwater storage in firn within the Greenland ice sheet, Nature Geoscience, 7, 95–98, https://doi.org/10.1038/ngeo2043, 2014.

Gilbert, E. and Kittel, C.: Surface Melt and Runoff on Antarctic Ice Shelves at 1.5°C, 2°C, and 4°C of Future Warming, Geophysical Research Letters, 48, e2020GL091 733, https://doi.org/10.1029/2020GL091733, 2021.

Gorelick, N., Hancher, M., Dixon, M., Ilyushchenko, S., Thau, D., and Moore, R.: Google Earth Engine: Planetary-scale geospatial analysis for everyone, Remote Sensing of Environment, 202, 18–27, https://doi.org/10.1016/j.rse.2017.06.031, 2017.

Hansen, J., Ruedy, R., Sato, M., and Lo, K.: GLOBAL SURFACE TEMPERATURE CHANGE, Reviews of Geophysics, 48, https://doi.org/10.1029/2010RG000345, 2010.

Hu, Z., Kuipers Munneke, P., Lhermitte, S., Izeboud, M., and van den Broeke, M.: Improving surface melt estimation over the Antarctic Ice Sheet using deep learning: a proof of concept over the Larsen Ice Shelf, The Cryosphere, 15, 5639–5658, https://doi.org/10.5194/tc-15-5639-2021, 2021.

Humphrey, N. F., Harper, J. T., and Pfeffer, W. T.: Thermal tracking of meltwater retention in Greenland's accumulation area, Journal of Geophysical Research: Earth Surface, 117, https://doi.org/10.1029/2011JF002083, 2012.

Jiahong, W., Jiancheng, K., Jiankang, H., Zichu, X., Leibao, L., and Dali, W.: Glaciological studies on the King George Island ice cap, South Shetland Islands, Antarctica, Annals of Glaciology, 27, 105–109, https://doi.org/10.3189/1998AoG27-1-105-109, 1998.

Kuipers Munneke, P., Ligtenberg, S. R. M., van den Broeke, M. R., van Angelen, J. H., and Forster, R. R.: Explaining the presence of perennial liquid water bodies in the firn of the Greenland Ice Sheet, Geophysical Research Letters, 41, 476–483, https://doi.org/10.1002/2013GL058389, 2014.

Kuipers Munneke, P., Luckman, A. J., Bevan, S. L., Smeets, C. J. P. P., Gilbert, E., van den Broeke, M. R., Wang, W., Zender, C., Hubbard, B., Ashmore, D., Orr, A., King, J. C., and Kulessa, B.: Intense Winter Surface Melt on an Antarctic Ice Shelf, Geophysical Research Letters, 45, 7615–7623, https://doi.org/10.1029/2018GL077899, 2018.

Lenaerts, J. T. M., Lhermitte, S., Drews, R., Ligtenberg, S. R. M., Berger, S., Helm, V., Smeets, C. J. P. P., van den Broeke, M. R., van de Berg, W. J., van Meijgaard, E., Eijkelboom, M., Eisen, O., and Pattyn, F.: Meltwater produced by wind-albedo interaction stored in an East Antarctic ice shelf, Nature Climate Change, 7, 58–62, https://doi.org/10.1038/nclimate3180, 2017.

Ligtenberg, S. R. M., Helsen, M. M., and van den Broeke, M. R.: An improved semi-empirical model for the densification of Antarctic firn, The Cryosphere, 5, 809–819, https://doi.org/10.5194/tc-5-809-2011, 2011.

MacDonell, S., Fernandoy, F., Villar, P., and Hammann, A.: Stratigraphic Analysis of Firn Cores from an Antarctic Ice Shelf Firn Aquifer, Water, 13, https://doi.org/10.3390/w13050731, 2021.

Macheret, Y., Otero, J., Navarro, F., Vasilenko, E., Corcuera, M., Cuadrado, M., and Glazovsky, A.: Ice thickness, internal structure and subglacial topography of Bowles Plateau ice cap and the main ice divides of Livingston Island, Antarctica, by ground-based radio-echo sounding, Annals of Glaciology, 50, 49–56, https://doi.org/10.3189/172756409789097478, 2009.

Miller, J. Z., Long, D. G., Jezek, K. C., Johnson, J. T., Brodzik, M. J., Shuman, C. A., Koenig, L. S., and Scambos, T. A.: Brief communication: Mapping Greenland's perennial firn aquifers using enhanced-resolution L-band brightness temperature image time series, The Cryosphere, 14, 2809–2817, https://doi.org/10.5194/tc-14-2809-2020, 2020.

Miège, C., Forster, R. R., Brucker, L., Koenig, L. S., Solomon, D. K., Paden, J. D., Box, J. E., Burgess, E. W., Miller, J. Z., McNerney, L., Brautigam, N., Fausto, R. S., and Gogineni, S.: Spatial extent and temporal variability of Greenland firn aquifers detected by ground and airborne radars, Journal of Geophysical Research: Earth Surface, 121, 2381–2398, https://doi.org/10.1002/2016JF003869, 2016.

Montgomery, L., Miège, C., Miller, J., Scambos, T. A., Wallin, B., Miller, O., Solomon, D. K., Forster, R., and Koenig, L.: Hydrologic Properties of a Highly Permeable Firn Aquifer in the Wilkins Ice Shelf, Antarctica, Geophysical Research Letters, 47, e2020GL089 552, https://doi.org/10.1029/2020GL089552, 2020.

Phillips, T., Rajaram, H., and Steffen, K.: Cryo-hydrologic warming: A potential mechanism for rapid thermal response of ice sheets, Geophysical Research Letters, 37, https://doi.org/10.1029/2010GL044397, 2010.

Picard, G., Sandells, M., and Löwe, H.: SMRT: an active–passive microwave radiative transfer model for snow with multiple microstructure and scattering formulations (v1.0), Geoscientific Model Development, 11, 2763–2788, https://doi.org/10.5194/gmd-11-2763-2018, 2018.

Scambos, T. A., Hulbe, C., Fahnestock, M., and Bohlander, J.: The link between climate warming and break-up of ice shelves in the Antarctic Peninsula, Journal of Glaciology, 46, 516–530, https://doi.org/10.3189/172756500781833043, 2000.

Scambos, T. A., Fricker, H. A., Liu, C. C., Bohlander, J., Fastook, J., Sargent, A., Massom, R., and Wu, A. M.: Ice shelf disintegration by plate bending and hydro-fracture: Satellite observations and model results of the 2008 Wilkins ice shelf break-ups, Earth Planet. Sci. Lett., 280, 51–60, https://doi.org/10.1016/j.epsl.2008.12.027, 2009.

Shi, J. and Dozier, J.: Radar backscattering response to wet snow, in: [Proceedings] IGARSS '92 International Geoscience and Remote Sensing Symposium, vol. 2, pp. 927–929, https://doi.org/10.1109/IGARSS.1992.578299, 1992.

Siegert, M., Atkinson, A., Banwell, A., Brandon, M., Convey, P., Davies, B., Downie, R., Edwards, T., Hubbard, B., Marshall, G., Rogelj, J., Rumble, J., Stroeve, J., and Vaughan, D.: The Antarctic Peninsula Under a 1.5°C Global Warming Scenario, Frontiers in Environmental Science, 7, https://doi.org/10.3389/fenvs.2019.00102, 2019.

Steger, C. R., Reijmer, C. H., van den Broeke, M. R., Wever, N., Forster, R. R., Koenig, L. S., Kuipers Munneke, P., Lehning, M., Lhermitte, S., Ligtenberg, S. R. M., Miège, C., and Noël, B. P. Y.: Firn Meltwater Retention on the Greenland Ice Sheet: A Model Comparison, Frontiers in Earth Science, 5, https://doi.org/10.3389/feart.2017.00003, 2017.

Stiles, W. H. and Ulaby, F. T.: The active and passive microwave response to snow parameters: 1. Wetness, Journal of Geophysical Research: Oceans, 85, 1037–1044, https://doi.org/10.1029/JC085iC02p01037, 1980.

https://doi.org/10.5194/tc-2022-127
Preprint. Discussion started: 4 October 2022

Travassos, J. and Simoes, J.: High-resolution radar mapping of internal layers of a subpolar ice cap, King George Island, Antarctica, Pesquisa Antártica Brasileira, 4, 57–65, 2004.

Trusel, L. D., Frey, K. E., Das, S. B., Karnauskas, K. B., Kuipers Munneke, P., van Meijgaard, E., and van den Broeke, M. R.: Divergent trajectories of Antarctic surface melt under two twenty-first-century climate scenarios, Nature Geoscience, 8, 927–932, https://doi.org/10.1038/ngeo2563, 2015.

Tsai, Y.-L. S., Dietz, A., Oppelt, N., and Kuenzer, C.: Remote Sensing of Snow Cover Using Spaceborne SAR: A Review, Remote Sensing, 11, https://doi.org/10.3390/rs11121456, 2019.

Turner, J., Lu, H., White, I., King, J. C., Phillips, T., Hosking, J. S., Bracegirdle, T. J., Marshall, G. J., Mulvaney, R., and Deb, P.: Absence of 21st century warming on Antarctic Peninsula consistent with natural variability, Nature, 535, 411–415, https://doi.org/10.1038/nature18645, 2016.

van den Broeke, M.: Strong surface melting preceded collapse of Antarctic Peninsula ice shelf, Geophysical Research Letters, 32, https://doi.org/10.1029/2005GL023247, 2005.

van Wessem, J. M., Reijmer, C. H., van de Berg, W. J., van den Broeke, M. R., Cook, A. J., van Ulft, L. H., and van Meijgaard, E.: Temperature and Wind Climate of the Antarctic Peninsula as Simulated by a High-Resolution Regional Atmospheric Climate Model, Journal of Climate, 28, 7306 – 7326, https://doi.org/10.1175/JCLI-D-15-0060.1, 2015.

van Wessem, J. M., Meredith, M. P., Reijmer, C. H., van den Broeke, M. R., and Cook, A. J.: Characteristics of the modelled meteoric freshwater budget of the western Antarctic Peninsula, Deep Sea Research Part II: Topical Studies in Oceanography, 139, 31–39, https://doi.org/10.1016/j.dsr2.2016.11.001, 2017.

van Wessem, J. M., van de Berg, W. J., Noël, B. P. Y., van Meijgaard, E., Amory, C., Birnbaum, G., Jakobs, C. L., Krüger, K., Lenaerts, J. T. M., Lhermitte, S., Ligtenberg, S. R. M., Medley, B., Reijmer, C. H., van Tricht, K., Trusel, L. D., van Ulft, L. H., Wouters, B., Wuite, J., and van den Broeke, M. R.: Modelling the climate and surface mass balance of polar ice sheets using RACMO2 – Part 2: Antarctica (1979–2016), The Cryosphere, 12, 1479–1498, https://doi.org/10.5194/tc-12-1479-2018, 2018.

van Wessem, J. M., Steger, C. R., Wever, N., and van den Broeke, M. R.: An exploratory modelling study of perennial firn aquifers in the Antarctic Peninsula for the period 1979–2016, The Cryosphere, 15, 695–714, https://doi.org/10.5194/tc-15-695-2021, 2021.

Veldhuijsen, S. B. M., van de Berg, W. J., Brils, M., Kuipers Munneke, P., and van den Broeke, M. R.: Characteristics of the contemporary Antarctic firn layer simulated with IMAU-FDM v1.2A (1979–2020), The Cryosphere Discuss. [preprint], in review, https://doi.org/10.5194/tc-2022-118, 2022.

https://doi.org/10.5194/tc-2022-127
Preprint. Discussion started: 4 October 2022

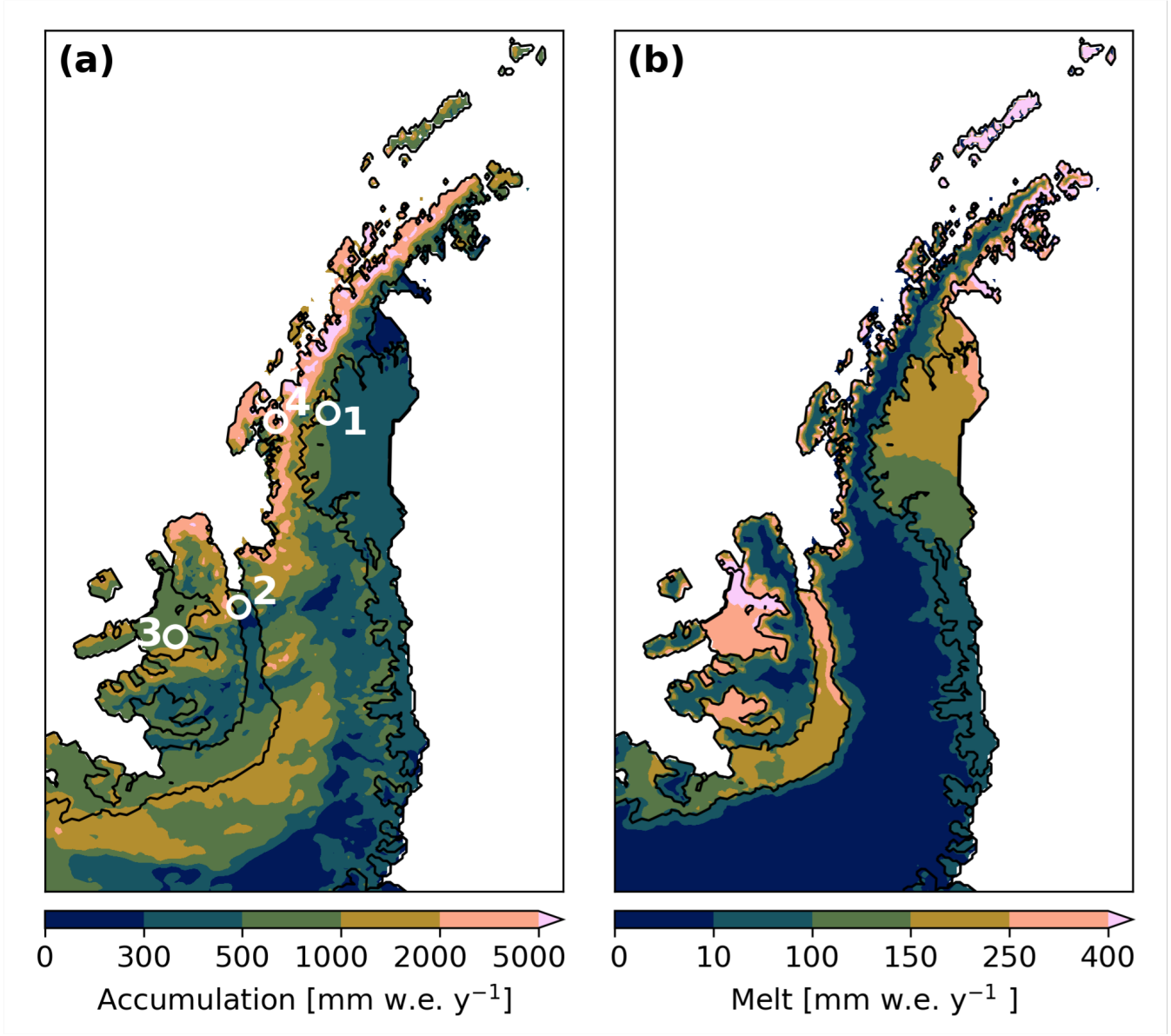

Figure 1. Antarctic Peninsula 2017-2020 average annual accumulation (a) and surface melt (b), from RACMO2.3p2 (updated from van Wessem et al. (2017)). Locations of the four backscatter time series are indicated by the numbered white circles in (a): Larsen C, George VI, Wilkins and Müller ice shelves.

https://doi.org/10.5194/tc-2022-127
Preprint. Discussion started: 4 October 2022

The Cryosphere
Discussions
Open Access
EGU

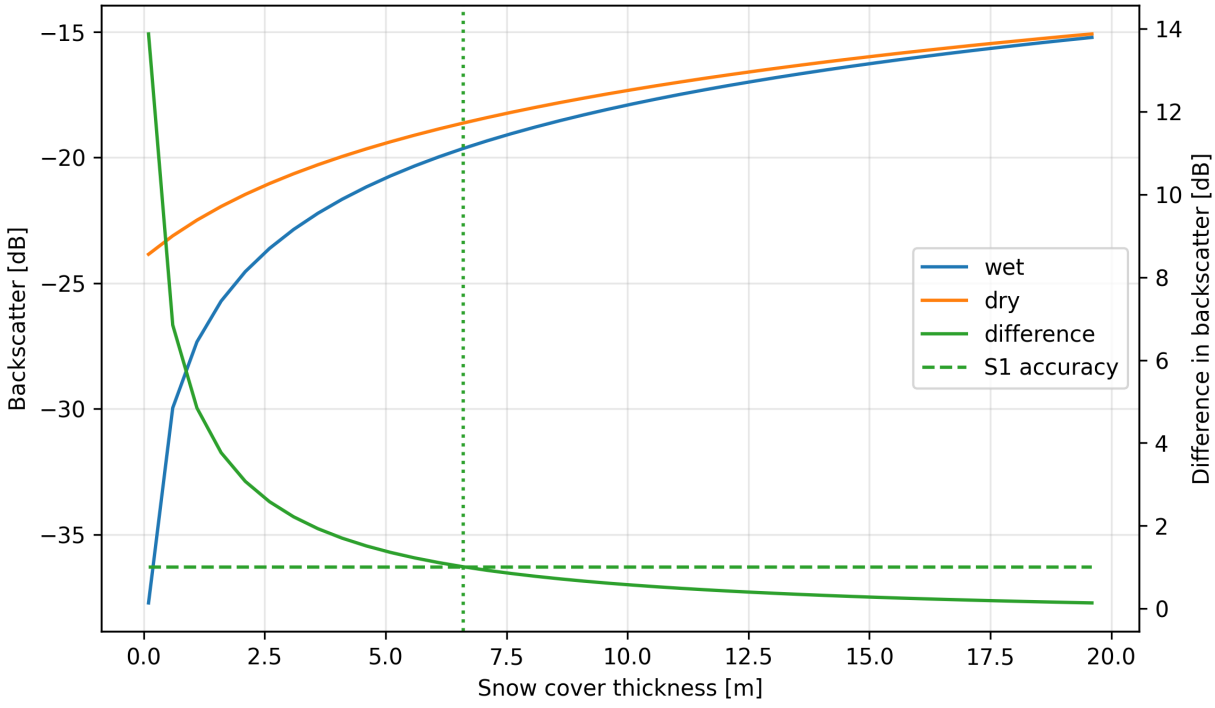

Figure 2. Left axis: The S1 backscatter signal in the presence of a wet (5 % LWC, blue) versus dry layer (orange) at different depths in the firn as simulated by the Snow Microwave Radiative Transfer (SMRT) model. Right axis: The solid green line shows the difference of both curves as compared to the radiometric accuracy of S1 (dashed green line).

https://doi.org/10.5194/tc-2022-127
Preprint. Discussion started: 4 October 2022

The Cryosphere
Discussions
Open Access
EGU

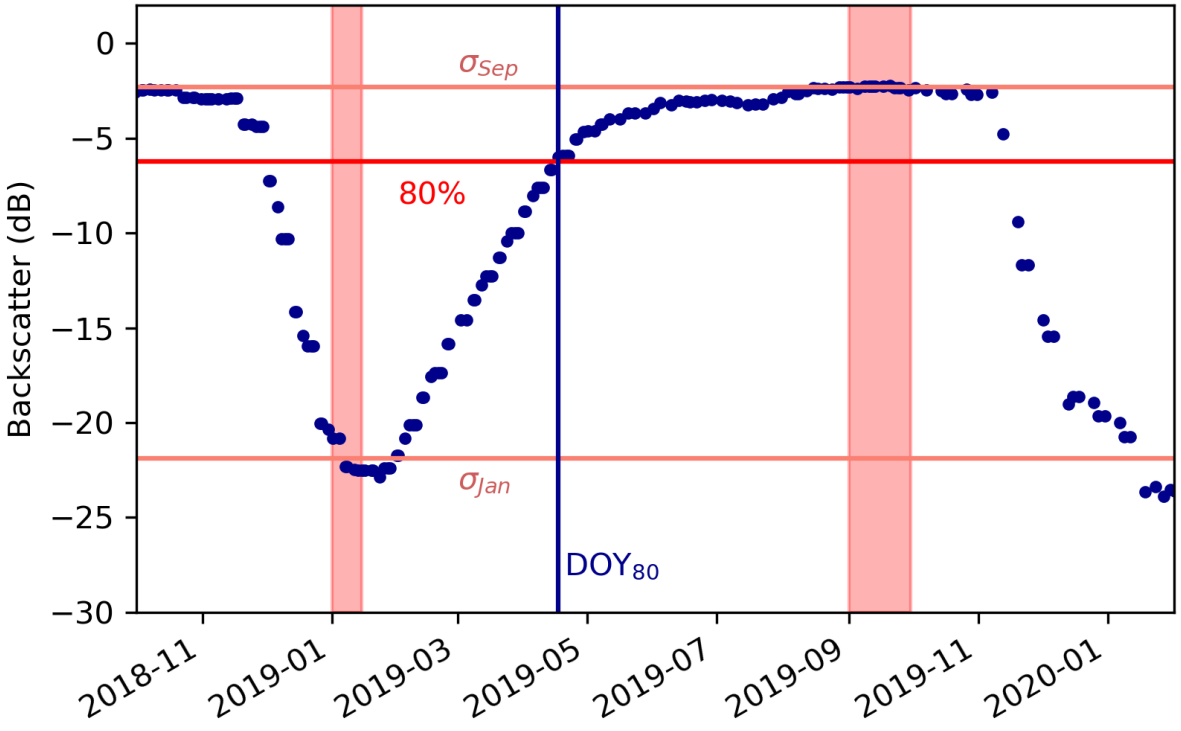

Figure 3. An illustration of the firn aquifer detection method presented in this study. Blue dots represent a backscatter time series, the periods 1-15 January and 1-30 September are highlighted as bars in salmon pink. Corresponding backscatter values and the 80 % threshold are indicated by horizontal lines. The vertical blue line shows the first day at which the 80 % threshold is exceeded (DOY_{80}), in this ideal case coinciding with the aquifer detection threshold $DOY_{80} \geq 105$.

https://doi.org/10.5194/tc-2022-127
Preprint. Discussion started: 4 October 2022

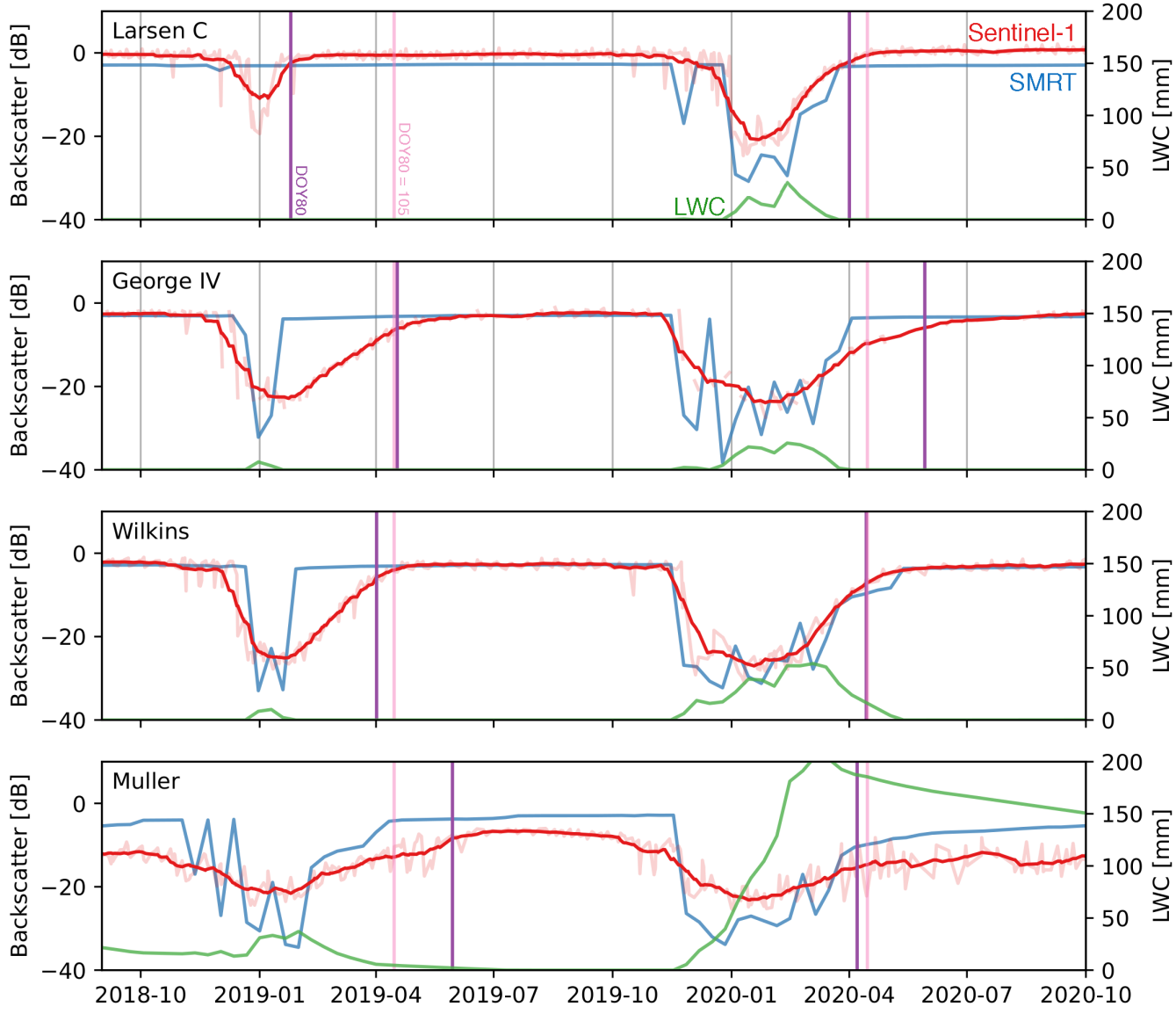

Figure 4. Time series for four example locations on (a) Larsen C, (b) George VI, (c) Wilkins and (d) Müller ice shelves (for locations see Fig. 1a) of observed and smoothed Sentinel-1 backscatter signal (red), modelled vertically (0-15 m depth) integrated IMAU-FDM liquid water content (LWC, green) and resulting modelled SRTM backscatter (blue). The coloured vertical lines represent the parameter DOY_{80} (purple) and threshold $DOY_{80} = 105$ (pink) for the respective location and year.

https://doi.org/10.5194/tc-2022-127
Preprint. Discussion started: 4 October 2022

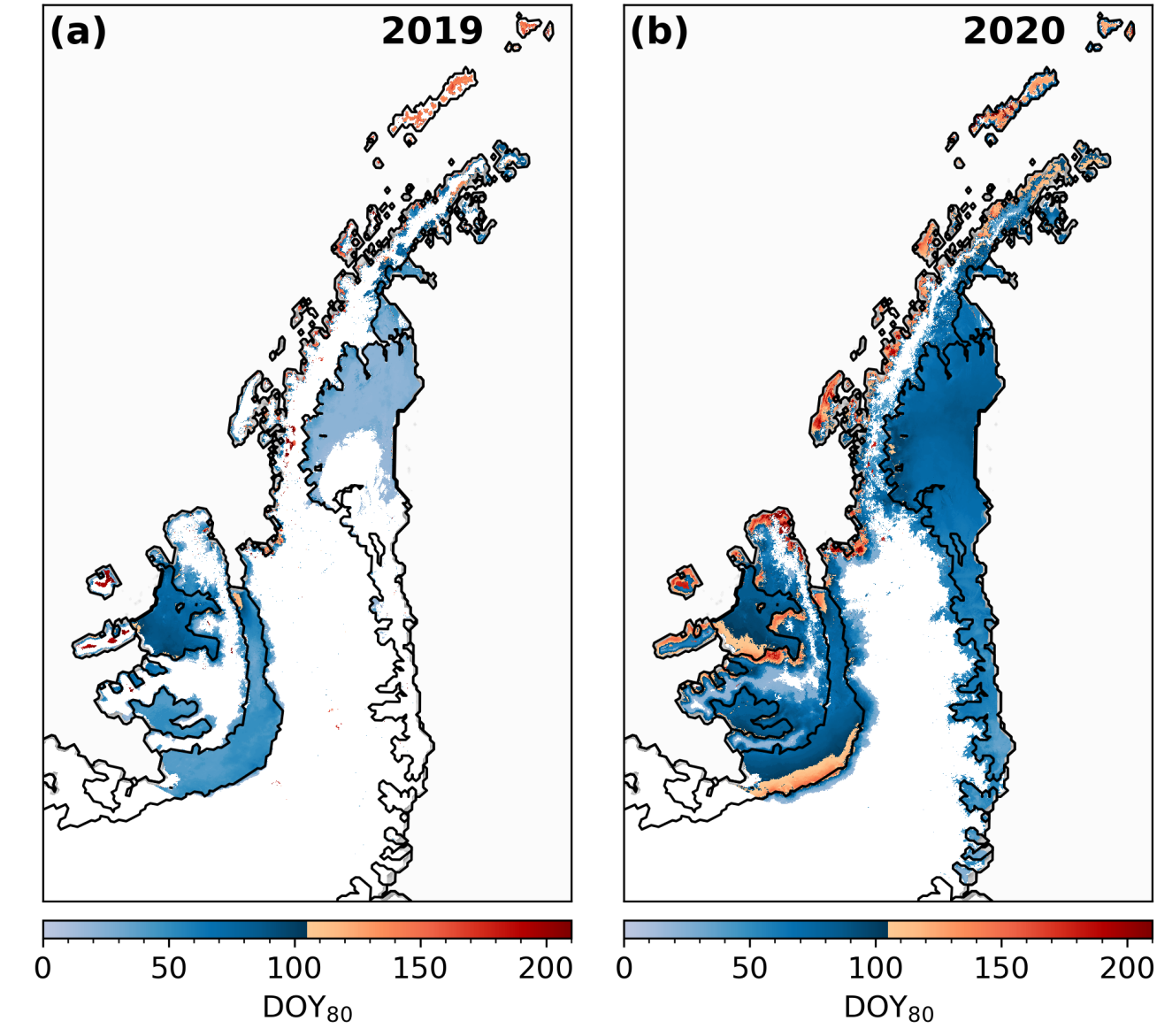

Figure 5. Day of the year (DOY) at which 80 % of σ_{Sep} with respect to σ_{Jan} is reached for the years (a) 2019 and (b) 2020. Locations where $\text{DOY}_{80} \geq 105$ (indicated by the red regions) are classified as S1 detected firn aquifers.

https://doi.org/10.5194/tc-2022-127
Preprint. Discussion started: 4 October 2022

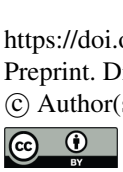

The Cryosphere
Discussions
Open Access
EGU

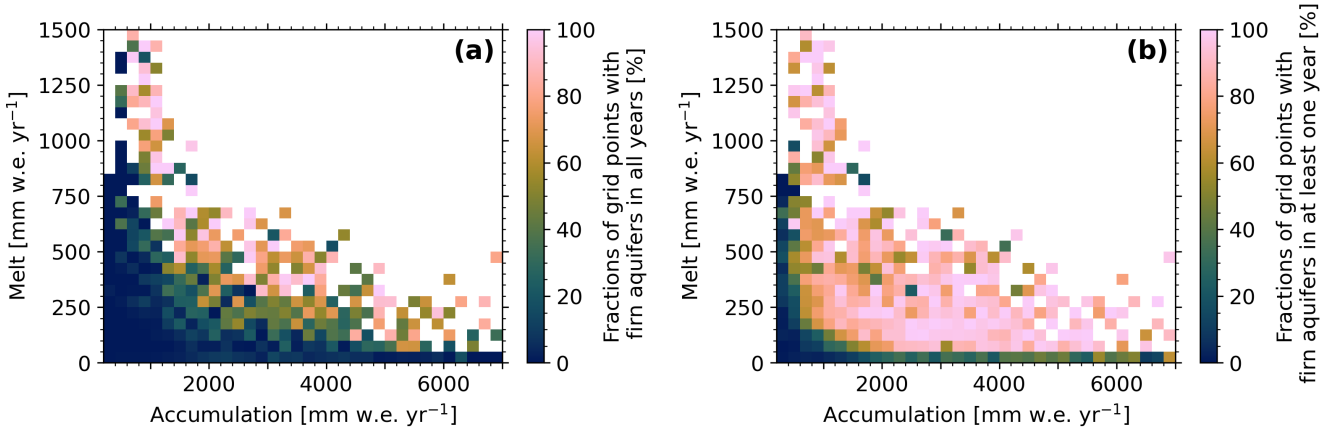

Figure 6. Percentage of S1 detected firn aquifer occurrences (a) in all years and in (b) at least one year over the period 2017-2020, as a function of annual surface melt (y-axis) and accumulation (x-axis) averaged over the period 2017-2020. RACMO2 grid cells are grouped in melt bins of 50 $\mathrm{mm\ w.e.\ y^{-1}}$ and accumulation bins of 200 $\mathrm{mm\ w.e.\ y^{-1}}$.

https://doi.org/10.5194/tc-2022-127
Preprint. Discussion started: 4 October 2022

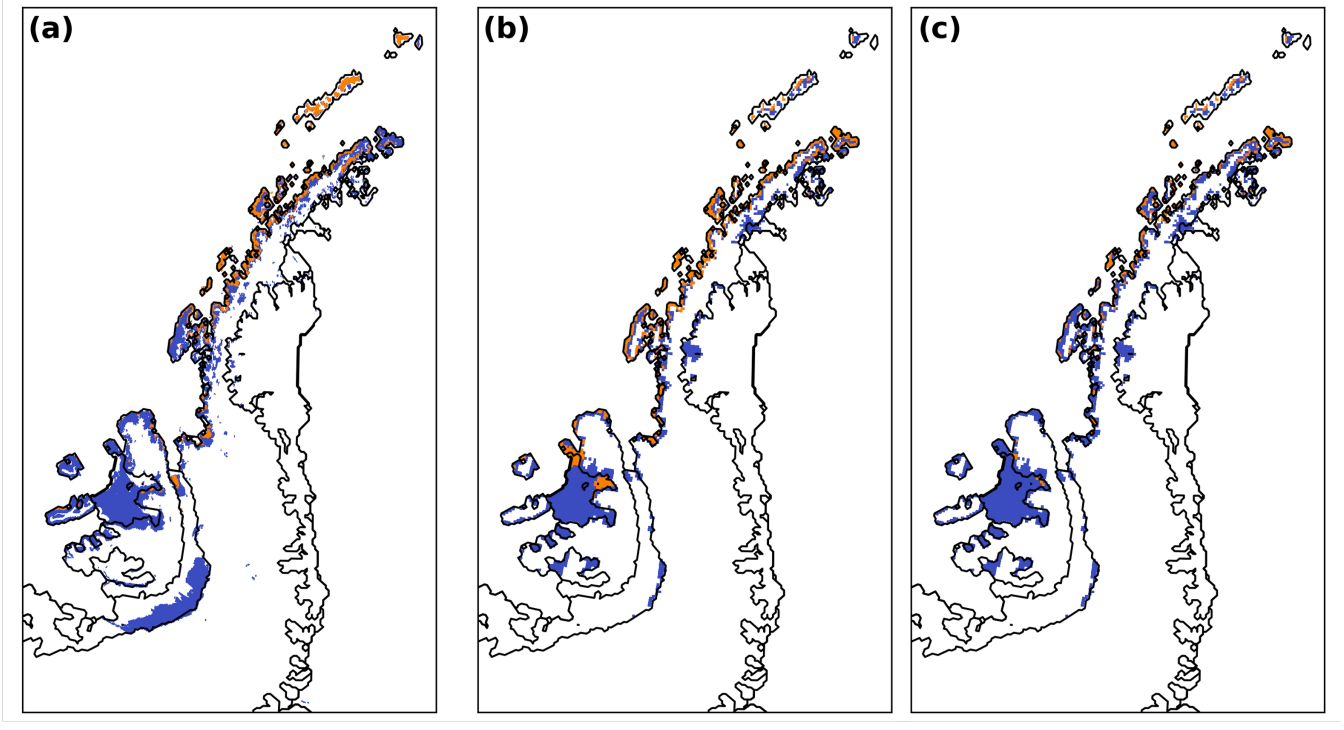

Figure 7. (a) Areas where S1 detects a firn aquifer in at least one of the four years (2017-2020, blue plus orange) or all of the three years with complete coverage (2018-2020, orange); (b) areas where IMAU-FDM simulates seasonal aquifer occurrence (2017-2020, blue plus orange) (any of the four April months LWC > 0) or perennial aquifer occurrence (2018-2020, orange, any of three September LWC > 0); (c) as in (b), but orange indicates LWC > 0 in all of three September months.